Energy 190 (2020) 116372

Contents lists available at ScienceDirect

Energy

journal homepage: www.elsevier.com/locate/energy

Modeling of heat transfer for energy efficiency prediction of solar receivers

J. Zhu [a], K. Wang [b], Z. Jiang [b], B. Zhua [a], H. Wu [c, *]

[a] National Key Laboratory of Science and Technology on Aero-Engine Aero-thermodynamics, Collaborative Innovation Center of Advanced Aero-Engine, School of Energy and Power Engineering, Beihang University, Beijing, 100191, China
[b] Institue of Engineering Thermophysics, Chinese Academy of Sciences, Beijing, 100190, China
[c] School of Engineering and Computer Science, University of Hertfordshire, Hartfield, AL10 9AB, United Kingdom

ARTICLE INFO

Article history:
Received 25 October 2018
Received in revised form
14 October 2019
Accepted 15 October 2019
Available online 16 October 2019

Keywords:
Solar receiver
Modeling
Energy efficiency
Metal foam
Radiation

ABSTRACT

In this article, a new heat transfer model for solar receivers with metal foam is developed for design optimization. The proposed model facilitates analysis of heat transfer processes in terms of forced convection, natural convection, heat conduction and radiation, accurately predicting the energy efficiency and percentage contribution of each form of heat loss. The results show good agreement between the predicted results and the experimental data. Specifically, sensitivity analysis is performed to predict the energy efficiency of solar receivers under different operating conditions. To explore the influence of inlet temperature, a series of simulations under high inlet temperature are carried out, resulting in poorer energy performance and heavier radiant heat loss. Non-radiant heat loss, however, accounts for less than 1.1% of the total energy loss in all cases. The results reveal that reduction of radiant loss is conducive to energy efficiency improvement.

© 2019 Elsevier Ltd. All rights reserved.

1. Introduction

Fossil fuel scarcity and the ever-worsening global warming nurture research and development of the renewable energy, among which solar energy is commonly recognized as one of the most promising candidates [1]. As one of the massive utilizing directions, the Concentrated Solar Power (CSP) system transfers solar energy into thermal energy, and finally into mechanical power (integration of the CSP system and Brayton micro-turbines is one example [2,3]). Solar receiver, one of the key components in CSP, works as a special energy exchanger to convert solar irradiation energy into thermal energy [4]. The thermal load of solar receivers could be significantly high, i.e. 1 MW is the central receiver system funded by the Ministry of Sciences and Technology of the People's Republic of China, set in Beijing in 2009 [5]. In the PEGASE (Production of Electricity by Gas Turbine and Solar Energy) project, the CNRS/PROMES laboratory developed a 4 MW pressurized air solar receiver based on compact heat exchanger technology [6]. ETH Zurich and Paul Scherrer Institute conducted a field test on a 42 m long full-scale solar receiver prototype installed on a 9 m-aperture solar trough concentrator. The efficiency of the receiver ranged from 29% to 45% with solar power input of 280 kW [7–9]. The results indicate high correlation between solar receivers' energy efficiency & total pressure loss and the system's efficiency and cost [10–12]. The collected thermal energy was transferred to other components in the system by circulating medium. To enhance heat transfer performance and reduce the dimension of the solar receiver, porous medium could be introduced as the collector medium. Metal foam is prevailing due to its high porosity (>95%), large specific surface area (>5000 m^{-1}), high mechanical strength and low cost [13,14]. The design optimization of the solar receiver is, however, still challenging due to the complexity of porous medium. Mendes et al. [15] proposed a simplified two-parameter model for effective thermal conductivity of open-cell porous foams. It was reported that the simplified model could predict the effective thermal conductivity of all the investigated structures in case of correct application of thermal conductivity ratio in each phase. By modeling differing virtual isotropic structures and performing 3-D direct numerical simulations, Kumar and Topin [16] generated a database of 2000 values about effective thermal conductivity. They studied the database to find the relationship between geometrical parameters and the effective thermal conductivity and built two models to predict the effective thermal conductivity, achieving excellent agreement between numerical and experimental data.

* Corresponding author.
E-mail address: h.wu6@herts.ac.uk (H. Wu).

https://doi.org/10.1016/j.energy.2019.116372
0360-5442/© 2019 Elsevier Ltd. All rights reserved.

Nomenclature

A_1	surface area of phase 1 (m^2)
A_g	area of quartz glass at the wavelength of visible light (m^2)
A_w	area of the inner cylinder wall of the front part of the Ni-foam (m^2)
C_{av}	average heat capacity of air inlet and outlet ($J \cdot kg^{-1}K^{-1}$)
$C_{p,h,1}$	average specific heat capacity of the air in hot end in phase 1($J \cdot kg^{-1}K^{-1}$)
C_{p3}	average specific heat capacity of the air in phase 3($J \cdot kg^{-1}K^{-1}$)
F_{fg}	radiation shape factor between foam and glass
F_{wg}	radiation shape factor between surface of inner cylinder and glass
h_{gi}	convective heat transfer coefficients of the inner surface of the quartz glass ($W/(m^2K)$)
h_{sf}	convective heat transfer coefficient of the Ni-foam ($W/(m^2K)$)
k_1	heat transfer coefficient for phase 1 ($W/(m^2K)$)
Q_r	energy absorbed by the receiver (J)
T_a	ambient temperature(°C)
T_g	temperature at the wavelength of visible light (°C)
T_o	temperature of outlet (°C)
ΔT_{min}	minimum between $(T_o - T_i)$ and $(T_4 - T_1)$ (°C)
α_g	absorbance at the wavelength of visible light
ε_f	emissivity of the Ni-foam
ε_w	emissivity of the inner cylinder wall of the front part of the Ni-foam
ρ_f	reflectivity of the Ni-foam
τ_g	transmittivity at the wavelength of visible light
A_f	area of the Ni-foam (m^2)
A_{sf}	surface area heat transfer coefficient of the Ni-foam (m^2)
A_c	shadow area of the concentrator(m^2)
$C_{p,c,1}$	average specific heat capacity of the air in cold end in phase 1($J \cdot kg^{-1}K^{-1}$)
C_{p2}	average specific heat capacity of the air in phase 2($J \cdot kg^{-1}K^{-1}$)
C_{p4}	average specific heat capacity of the air in phase 4 ($J \cdot kg^{-1}K^{-1}$)
F_{fw}	radiation shape factor between foam and the wall of the inner cylinder
G	instantaneous solar radiation density (W/m^2)
h_{go}	convective heat transfer coefficients of the outer surface of the quartz glass ($W/(m^2K)$)
I_b	energy entering the solar receiver (J)
$\dot{m}$	mass flow rate (kg/s)
T_{34}	average of temperature T_3 and T_4(°C)
T_f	temperature of the Ni-foam (°C)
T_i	temperature of inlet (°C)
ΔT_{max}	maximum between $(T_o - T_i)$ and $(T_4 - T_1)$ (°C)
T_w	temperature of the inner cylinder wall of the front part of the Ni-foam (°C)
$\alpha_g^{'}$	absorbance of quartz glass under long wave
$\varepsilon_g^{'}$	emissivity of quartz glass under long wave
η_c	specular reflection efficiency of the concentrator
σ	blackbody radiation intensity($5.67x10^{-8}$ $W/(m^2K^4)$)
Φ_1	specific heat absorbed by the air in phase 1 (W)

The porous medium used in solar receivers has also been investigated. Buck et al. [17] conducted a performance test and retrofitted a receiver with new secondary concentrator. Several configurations of solar-hybrid gas turbine cycles in the low-medium power range were examined in terms of performance and cost. Albanakis et al. [18] tested different materials of porous medium and evaluated the receiver performance under varying operating conditions, demonstrating that Nickel foam bears better thermal property than the other foams. Michailidis et al. [19] employed the Ni-foam as porous medium in solar receivers and identified that the efficiency of the receiver depended on the geometrical parameters of the metal foam.

As experimental investigations cost high and last short, numerical simulation also plays an important role in design and optimization phase. He et al. [20] established a coupled heat transfer model based on the Monte Carlo Ray Trace (MCRT) and Finite Volume Method (FVM) to predict the thermal behaviour in a parabolic trough solar receiver system. The average relative error was identified less than 2% by comparing the predicted outlet temperature with that of the experimental results. Wu et al. [21] presented a coupled heat transfer model to calculate the unsteady heat conduction of porous medium in solar receivers, which was proved as an efficient tool for receiver performance prediction. Chen et al. [22] examined the effect of various combinations of porosities and pore-sizes of porous medium on heat transfer performance. Hischier et al. [23] proposed a theoretical receiver model and conducted numerical calculation on a solar receiver used in a power generation system with combined Brayton-Rankine cycles [24]. Parametrical studies on temperature distribution and thermal efficiency have also been performed. The optimum predicted configuration was set and corresponding experimental investigations conducted [23]. After repeated design and test [25], a complete receiver with an output power of 35 kW was constructed and tested [26]. In addition, Lim et al. [27] designed a model for a tube-typed receiver by studying heat transfer characteristics and pressure drop characteristics based on discussion of the model and the optimum design. Weigal [28] also established a receiver model to analyze the measured efficiency value of solar receivers, which was lower than the designed one. Mortazavi [29] developed multiscale modeling techniques to explore the thermal management efficiency of rechargeable batteries by employing paraffin composite structures.

It can be revealed from the above studies that modeling of heat transfer in solar receivers is important for development and optimization of the component as well as the energy system. To the best knowledge of the authors, few research has been reported to explore the heat transfer process in solar receivers with porous medium taking forced convection, natural convection, heat conduction and radiation into account. Currently, a new heat transfer model for solar receivers with porous medium has been developed for design optimization, which has been validated by experimental data. Corresponding sensitivity analysis has also been carried out, providing reference for solar receiver design improvement. It is expected that the proposed model will be highly conducive to accurate prediction of the efficiency of heat exchanger under differing operating conditions.

2. Establishment of heat transfer analyzing model

2.1. Configuration of solar receiver

Fig. 1 presents a pressurized volumetric solar receiver in current CSP system, Fig. 1(a) a cross-sectional view of the receiver, and Fig. 1(b) a 3D view of the model. The advantage of the pressurized volumetric solar receiver lies in its high outlet air temperature and high thermal efficiency, although cooling of the light-incident glass and the flow balance in the heat absorbing core were two challenging problems in the process. The light-incident glass is made of quartz glass that can endure the maximum temperature of 1200 °C, yet when the concentrated solar directly focused on the glass, mechanical failure of cooling may occur. As a solution, the inlet air with relatively low temperature flowed through the glass as coolant, both extending the receiver's service life and reducing the probability of mechanical failure. Therefore, a large 50 mm-diameter inlet tube was adopted, into which the pressurized air was injected and then separated into three 20 mm-diameter branches. Welded on the back-side flange of the pressure cavity, the three smaller tubes were equally distributed in circumferential direction. Then, the air flowed through the gap between the internal and external cavities to the front region of the chamber and impinged onto the quartz glass.

The main part of the receiver is 400 mm in diameter and 360 mm in height. The concentrated solar radiation (CSR) passed through the quartz glass and heated the absorbing core, which was made of Nickel foam that could endure the maximum temperature of 1453 °C. To increase the absorbing capacity, a 65 mm-thick Nickel foam with the PPI (Pores per Inch) value of 75 and pore diameter of 0.34 mm was selected. Normally, smaller pore diameter entails larger heat transfer area and higher mean heat transfer coefficient. At last, to minimize heat loss, the receiver was surrounded by Aluminum silicate whose heat conductivity coefficient reached 0.06 W/(m·°C).

2.2. Energy balance equation

A simplified model (Fig. 2) was established to calculate the steady-state heat transfer efficiency by analyzing heat loss. It is assumed that the solar radiation transmitted through the quartz glass window into the solar receiver's cavity is entirely irradiated

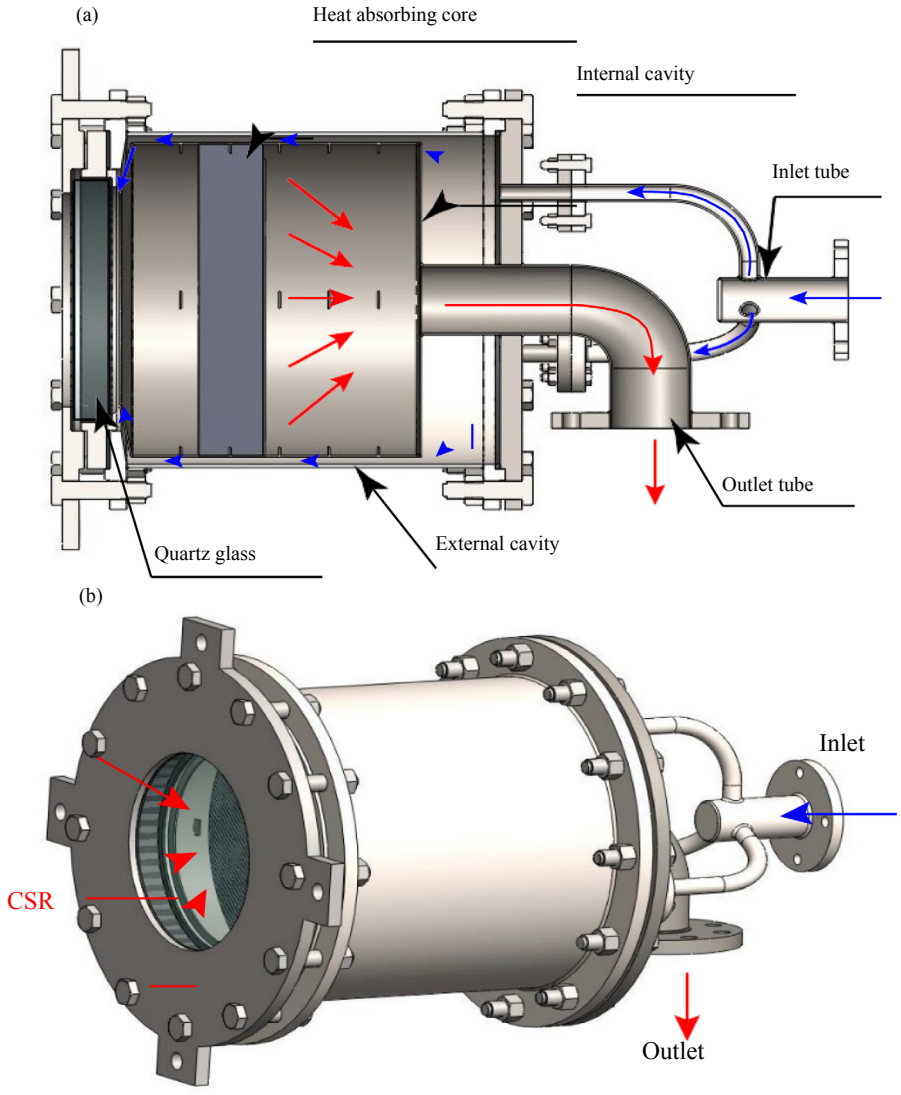

Fig. 1. (a) Cross-section view of the receiver. (b) 3D view of the pressurized volumetric solar receiver.

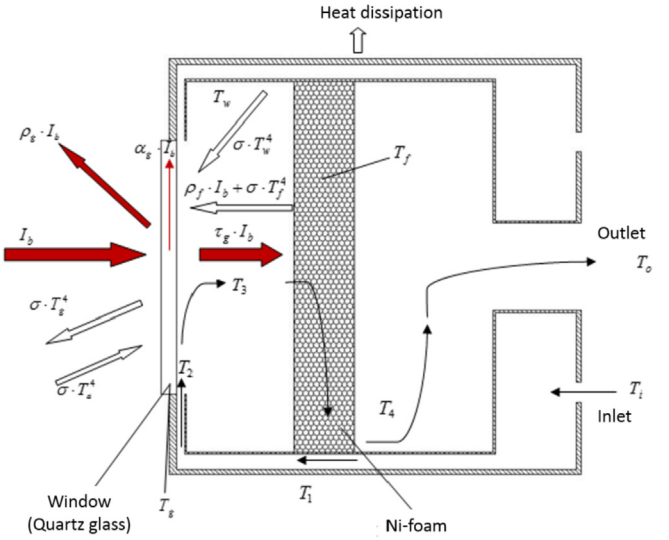

Fig. 2. Simplified heat transfer model.

on the surface of the metal foam, which is a uniform medium, and the air constitutes ideal gas. The heat transfer process is analyzed from the following five steps.

Initially, in the process of $T_i \rightarrow T_1$, the cooling air flows into the inlet and is heated by the foam through the wall of inner cylinder. Therefore, the enthalpy balance is expressed as:

$$\varnothing_1 = C_{p,c,1} \cdot \dot{m} \cdot (T_1 - T_i) = C_{p,h,1} \cdot \dot{m} \cdot (T_4 - T_o) \tag{1}$$

$$\Phi_1 = k_1 A_1 \frac{\Delta T_{\max} - \Delta T_{\min}}{Ln \frac{\Delta T_{\max}}{\Delta T_{\min}}} \tag{2}$$

Φ_1 represents the specific heat absorbed by the air, $C_{p,c,1}$ and $C_{p,h,1}$ the average specific heat capacity of the air between cold and hot ends, $\dot{m}$ mass flow rate, T_o and T_i outlet and inlet temperature, k_1 heat transfer coefficient, A_1 the surface area of phase 1, $\Delta T_{\max}$ the maximum temperature difference between $(T_o - T_i)$ and $(T_4 - T_1)$, and $\Delta T_{\min}$ the minimum temperature difference.

Then, in the process of $T_1 \rightarrow T_2$, the heated air transfers heat through the wall of inner cylinder. The wall is both heated up by metal foam radiation and reflection of the metal foam solar radiation. Thus, the following relations can be established.

$$C_{p2} \cdot \dot{m} \cdot (T_2 - T_1) = h_w A_2 \frac{(T_w - T_1) - (T_w - T_1)}{ln\left(\frac{T_w - T_1}{T_w - T_1}\right)} \tag{3}$$

$$C_{p2} \cdot \dot{m} \cdot (T_2 - T_1) = \varepsilon_w F_{fw} \left\{ \varepsilon_f A_f \sigma \left[\left(T_f + 273\right)^4 - (T_2 + 273)^4 \right] + \rho_f \tau_g \eta_c A_c G \right\} \tag{4}$$

where C_{p2} stands for the average specific heat capacity of the air in the second process, ε_w, T_w and A_w the emissivity, temperature and area of inner cylinder wall in the front part of the foam, ρ_f, ε_f, T_f and A_f the emissivity, temperature and area of the Ni-foam, F_{fw} the radiation shape factor between the foam and the wall of inner cylinder, and σ the blackbody radiation intensity valued 5.67 X 10^{-8} W/(m^2·°C).

In the succeeding process of $T_2 \rightarrow T_3$, the air flows through the outflow channel and flushes the inner surface of the quartz glass towards the window center, exchanging heat with the glass surface. Aside from the internal convective heat transfer on the inner wall of the glass, the natural convection on the outer wall, the radiation from incident sunlight, the reflected radiation from the foam, and the radiation from the inner cylinder surface are also dealt with in the proposed model.

$$C_{p3} \cdot \dot{m} \cdot (T_3 - T_2) = A_g h_{gi} \frac{(T_g - T_2) - (T_g - T_3)}{ln\left(\frac{T_g - T_2}{T_g - T_3}\right)} \tag{5}$$

$$\begin{aligned} &\alpha_g I_b + \alpha_g' F_{fg} \left[\rho_f \tau_g I_b + \varepsilon_f A_f \sigma \left(T_f^4 - T_g^4 \right) \right] + \alpha_g' F_{wg} \varepsilon_w A_w \sigma \left(T_w^4 - T_g^4 \right) \\ &= \varepsilon_g' A_g \sigma \left(T_g^4 - T_a^4 \right) + A_g h_{go} (T_g - T_a) \\ &\quad + A_g h_{gi} \frac{(T_g - T_2) - (T_g - T_3)}{Ln\left(\frac{T_g - T_2}{T_g - T_3}\right)} \end{aligned} \tag{6}$$

where C_{p3} signifies the average specific heat capacity of the air in the third process, α_g, τ_g, T_g, A_g the absorbance, transmissivity, temperature and area of the quartz glass at the wavelength of visible light, α_g', ε_g' the absorbance and emissivity of the quartz glass under the long wave, F_{fg} the radiation shape factor between the foam and glass, F_{wg} the radiation shape factor between the surface of inner cylinder and glass, T_a the ambient temperature, and h_{go}, h_{gi} the convective heat transfer coefficients of the outer and inner surface of the quartz glass.

In the fourth process of $T_3 \rightarrow T_4$, the air flows into the metal foam and transfers the heat energy after flushing the inner surface of the glass,

$$C_{p4} \cdot \dot{m} \cdot (T_4 - T_3) = A_{sf} h_{sf} \left(T_f - T_{34} \right) \tag{7}$$

in which C_{p4} means the average specific heat capacity of the air in this process, A_{sf} and h_{sf} the surface area and convective heat transfer coefficient of the metal foam, T_{34} the average value of temperature between T_3 and T_4. The last process of $T_4 \rightarrow T_o$ is identical with the first one $T_i \rightarrow T_1$. The specific surface area of the metal foam A_{sf} is determined by the formula used in literature [14],

$$A_{sf} = \frac{3\pi d_f}{(0.59 d_p)^2} [1 - \exp(-((1-\varphi)/0.04))] \tag{8}$$

where d_f denotes the thickness of the metal foam, which can be measured directly and calculated by the following formula,

$$\frac{d_f}{d_p} = 1.18 \sqrt{\frac{1-\varphi}{3\pi}} \frac{1}{1 - \exp(-((1-\varphi)/0.04))} \tag{9}$$

Radiant loss, convective loss and heat dissipative loss are the major heat loss forms of the entire receiver. Radiant loss concerns the loss of radiation from the quartz glass window and the chamber. Most of the convective loss is generated by the natural convection on the outer surface of the quartz glass window, while heat dissipative loss by the conduction through the insulations. Therefore, heat loss can be expressed as:

$$\begin{aligned} Q_{loss} = {} & Q_{glass,emission} + Q_{glass,reflec\tan ce} + Q_{foam,emission} \\ & + Q_{foam,reflec\tan ce} + Q_{wall,emission} + Q_{convection} + Q_{conduction} \end{aligned} \tag{10}$$

Since the thermal conductivity of the quartz glass is 1.46 w/(m K), the thermal loss is small enough to be ignored. Other forms of heat loss can be calculated as follows,

$$Q_{glass,emission} = \varepsilon_g' A_g \sigma \left(T_g^4 - T_a^4\right) \tag{11}$$

$$Q_{glass,reflec\ tan\ ce} = \rho_g I_b \tag{12}$$

$$Q_{foam,emission} = \tau_g' F_{fg} \varepsilon_f A_f \sigma \left(T_f^4 - T_a^4\right) \tag{13}$$

$$Q_{foam,reflec\ tan\ ce} = \tau_g' F_{fg} \rho_f I_b \tag{14}$$

$$Q_{wall,emission} = \tau_g' F_{wg} \varepsilon_w A_w \sigma \left(T_w^4 - T_a^4\right) \tag{15}$$

$$Q_{convection} = A_g h_{go} \left(T_g - T_a\right) \tag{16}$$

Finally, the efficiency of the receiver is expressed as,

$$\eta_{receiver} = \frac{I_b - Q_{loss}}{I_b} \tag{17}$$

To calculate the efficiency of the receiver, parameters in the formulas should be determined, of which the most critical ones are T_g, T_f, and T_w.

2.3. Heat transfer calculation

To examine the heat transfer process and calculate the efficiency of the receiver, the essential parameters in the above formulas should be obtained.

The radiant performance parameters of the quartz glass at visible and long wavelengths are obtained [30]. Due to the large porosity of mental foam, the effective emissivity is taken as 0.95. Being made of stainless steel, the surface of inner cylinder has emissivity of about 0.8 in the case of heavy oxidation. Relevant radiant performance parameters are summarized in Table 1.

Geometrical parameters, including the surface area of each component and the radiation shape factors, are also required. The area values are easy to be determined. As calculation of shape factors is complex, the geometrical structure between the metal foam surface and the flat window are simplified into two coaxial parallel discs; therefore, the radiation shape factors of the structure, F_{fg}, can be expressed as,

$$R_1 = \frac{r_1}{L},\ R_2 = \frac{r_2}{L},\ S = 1 + \frac{1 + R_2^2}{R_1^2},\ F_{1,2} = \frac{1}{2}\left\{S - \left[S^2 - 4(r_2/r_1)^2\right]^{1/2}\right\} \tag{18}$$

in which r_1 and r_2 represent the radius of the first and second disc, and L the distance between the discs. Similarly, the shape factors F_{fw} and F_{wg} can be determined. The calculated geometric parameters are summarized in Table 2.

Table 1
Radiant performance parameters.

		emissivity	reflectivity	transmissivity
Quartz glass	Visible wave	0.013	0.136	0.851
	Long wave	0.326	0.125	0.549
Mental foam		0.95	0.05	/
The surface of inner cylinder		0.8	0.2	0

Table 2
Results of geometric parameters.

Parameter	A_f	A_g	A_w	F_{fg}	F_{fw}	F_{wg}
Value	0.1041m^2	0.0491m^2	0.1788m^2	0.3171	0.4340	0.1340

The first and second processes are assumed as forced convection in pipe. The outer surface of the glass for the third process is assumed as large-space natural convection, while the inner surface as forced convection on a flat plate. Besides, the fourth process is accepted as convective heat transfer in the metal foam. Therefore, the Nusselt number of the convective heat transfer in the first process, that is Nu_1, could be determined with the Gnielinski Formula [31] expressed below,

$$Nu_1 = \frac{(f/8)(\mathrm{Re} - 1000)\mathrm{Pr}_f}{1 + 12.7\sqrt{f/8}\left(\mathrm{Pr}_f^{2/3} - 1\right)}\left[1 + \left(\frac{d}{l}\right)^{2/3}\right]c_t \tag{19}$$

$$c_t = \left(\frac{T_f + 273}{T_w + 273}\right)^{0.45},\ \frac{T_f + 273}{T_w + 273} = 0.5 \sim 1.5 \tag{20}$$

$$f = (1.82\lg\mathrm{Re} - 1.64)^{-2} \tag{21}$$

where l is the tube length and f the Darcy resistance coefficient. Similarly, the convective heat transfer coefficient between the air and the surface of inner cylinder in the second process, i.e. Nu_2, can be calculated with Gnielinski Formula as well.

In the third phase, the Nusselt number of the natural convection on the outer surface can be computed as,

$$Nu_{3,m} = C(Gr \cdot \mathrm{Pr})_m^n \tag{22}$$

in which the values of C, m and n depend on the Grashof number cited in Ref. [31]. The Nusselt number of the forced convection on the inner surface of the quartz glass ($Nu_{3,l}$) is calculated with the heat transfer correlation of the thin layer flow of isothermal plate as,

$$Nu_{3,l} = 0.664\mathrm{Re}_l^{1/2}\mathrm{Pr}^{1/3} \tag{23}$$

The convective heat transfer coefficient between the air and the metal foam in the fourth phase is determined by the Rukavuscass formula [32] listed below,

$$Nu_4 = \begin{cases} 0.74\mathrm{Re}^{0.4}\mathrm{Pr}^{0.37}, 1 \le \mathrm{Re} \le 4 \\ 0.52\mathrm{Re}^{0.5}\mathrm{Pr}^{0.37}, 4 \le \mathrm{Re} \le 10^3 \\ 0.26\mathrm{Re}^{0.6}\mathrm{Pr}^{0.37}, 10^3 \le \mathrm{Re} \le 2 \times 10^5 \end{cases} \tag{24}$$

Solutions of T_g, T_f and T_w depend on individual phases' air temperature. In phase 1, T_1 and T_4 can be calculated through calibration calculation steps of the receiver since T_i, T_o, k_1 and A_1 are known. Therefore, there are only five unknown temperature values: T_2, T_3, T_g, T_f, T_w, which can be simultaneously solved through Eqs. (3)–(7) with iterative method. As all the unknown parameters in Eqs. (11)–(16) have been determined, the heat loss and efficiency of the solar receiver can be solved through Eqs. (10) and (17).

3. Results and discussions

3.1. Model validation

The energy source of heat exchanger is mainly solar radiation,

and the energy entering the solar receiver can be calculated when the technical parameters of the concentrator are known,

$$I_b = \eta_c A_c G \tag{25}$$

where I_b represents the energy entering the solar receiver, η_c and A_c the specular reflection efficiency and shadow area of the concentrator, and G the instantaneous solar radiation density.

The net energy absorbed by the receiver can be calculated by the temperature difference between the inlet and outlet of air flow,

$$Q_r = C_{av} \cdot \dot{m} \cdot (T_o - T_i) \tag{26}$$

where Q_r is the energy absorbed by the receiver, and C_{av} the average heat capacity of air inlet and outlet.

Therefore, the thermal efficiency of the solar receiver in the experiment can be obtained by calculating the ratio between the heat absorbed by the receiver and the heat entering the receiver:

$$\eta_{receiver} = \frac{Q_r}{I_b} = \frac{\dot{m} C_{av} (T_o - T_i)}{\eta_c A_c G} \tag{27}$$

Eq. (27) is for calculating the experimental error of the receiver's heat efficiency, which reaches $\mp 5.632\%$ according to the measuring instrument accuracy and error calculation formula of indirect measurement.

The existing solar receiver is located at Jianggan district, Hangzhou, Zhejiang province, China, with longitude of 120.222°and latitude of 30.364°. As presented in Fig. 3, the experimental system of the solar receiver is composed of five subsystems: gas source, dish-shaped solar concentration part, solar receiver, pipeline system and data acquisition system. The air compressed by air pump flows into the receiver through pipe, and then the heated pressurized air is exhausted into the atmosphere. Data collection points are arranged in the pipe as well as the receiver, whose working pressure is five times higher than the atmosphere pressure. To limit the flow temperature variation between inlet and outlet (less than 600 °C), the minimum air flow rate is set around 0.04 kg/s, the projected area of the solar concentrator around 44 m^2, and the optical efficiency 86.45%. Data acquisition system is designed for collecting and storing data of temperature, pressure, volume flow and direct solar radiant intensity transmitted through each measurement point in the solar receiver. Temperature measurement points are set on the outer wall, front & rear cover and the wall near the outlet (for correcting the outlet temperature error caused by thermal radiation). A pressure measurement point is also arranged near the flow measurement point. A vortex flowmeter is adopted to measure the volumetric flow of air, whose mass flow rate is obtained by virtue of the temperature and pressure data near the flowmeter. The experiment was conducted on November 5 and 6, 2015. The amount of radiation was estimated based on the solar radiation model mentioned in Ref. [33]. The direct solar radiation during daytime fluctuated considerately due to the heavy cloud, thus only the data collected on November 6 were selected. Values of air mass flux, efficiency and temperature of the outlet versus local time are shown in Fig. 4.

Due to a sudden change of cloud cover and solar radiation intensity, the response lag of the measuring system may lead to an error: the sudden instantaneous efficiency is greater than 1 (for example, the efficiency measured at 12:47 to 12:52 is greater than 1). The efficiency measured at the rest time fluctuates in the range of 30%–85%. It can be observed that the data collected from 11:12 to 11:45 is relatively stable, thus is highlighted with yellow box in Fig. 4 for model validation. The air mass flux in this region reaches around 0.043 kg/s (2 Nm^3/min), and corresponding energy efficiency 81.5%. The temperature values obtained in the experiment are used to calculate thermal parameters according to Eqs. (18)–(24). The results are shown in Table 3.

As Eqs. (3)–(7) are nonlinear, matrix operation is replaced by iteration for easy calculation. The optimization algorithms used are quasi-Newton method and general global optimization method. Table 4 displays the calculated temperature at each state.

Heat losses of the solar receiver could be calculated with Eqs.(10)–(15). Conductive losses were estimated according to the experimentally measured temperature of the outer surface of the receiver, where several temperature sensors were arranged. The estimated value of the heat dissipative loss provided by the experimental data was 2%. The total heat loss and energy efficiency were solved according to Eqs. (8) and (9). Specifically, the measured

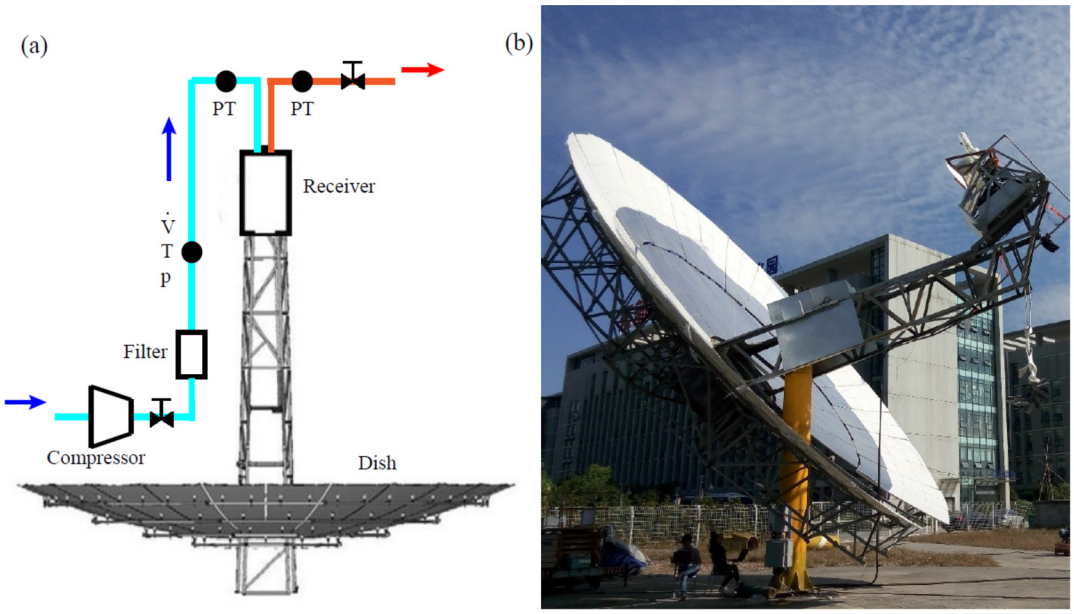

Fig. 3. (a) Schematic diagram of the experimental system. (b) Photo of the experimental system.

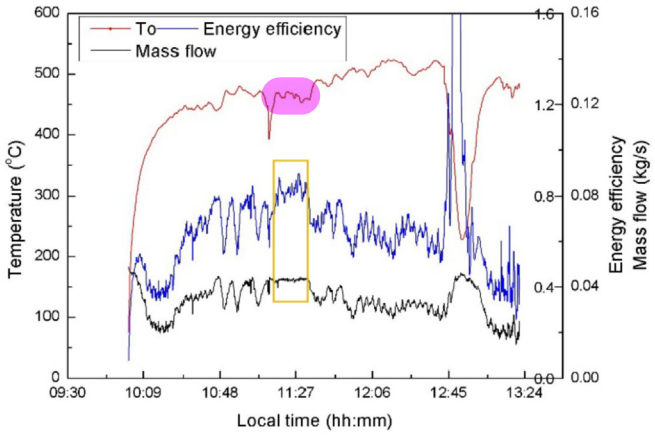

Fig. 4. Variation of air mass flux, efficiency and temperature of the outlet.

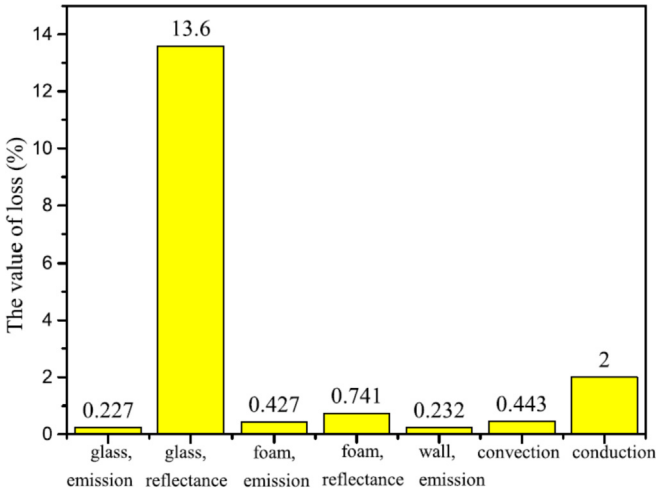

Fig. 5. Shares of heat losses in the solar receiver.

Table 3
Summary of thermal parameters.

parameter	k_1	h_w	h_{gi}	h_{go}	h_{sf}	A_{sf}
value	9.7	20.7	39	10	450	2023

Table 4
Temperature in each phase.

Temperature	T_1	T_2	T_3	T_4	T_f	T_w	T_g
Value	77.0	90.9	97.0	495.8	300.5	257.6	233.1

energy efficiency was 81.5%, while the predicted one was around 82.3%, suggesting good agreement between the two. Therefore, the proposed model is capable of accurately predicting the energy efficiency of the system.

3.2. Heat loss analysis

The experimental data and model prediction were identical on the condition of several assumptions and approximations, thus more parameters should be referenced for further validation. Heat loss plays an important role in heat transfer experiments, which in turn increases the uncertainty of the experimental data, intensifying the necessity of heat loss analysis. The limitations of this simplified heat transfer model are summarized as follows. At first, obtained in the simplified geometry that was slightly different from the currently adopted geometry, all the equations used in the model are of empirical nature. Then, adoption of lumped temperature for each solid part leads to ignorance of the temperature variation inside each single component. In terms of radiation calculation, only the first-time reflection is considered. Besides, this model merely concerns the important features of the system that may substantially influence the heat transfer process. Moreover, it is assumed by this model that the air flows smoothly through the metal foam in phase 4. In particular, for calculation simplification, arithmetic mean value of temperature difference is utilized instead of instant temperature difference.

Despite the limitations, the heat loss results can still be used to analyze the performance of the current receiver. As described above, heat loss mainly consists of radiant loss, convective loss and conductive loss caused by heat dissipation. The share of each form of heat loss is illustrated in Fig. 5. It can be observed that the loss induced by the reflection on the quartz glass window constitutes the major part of heat losses, accounting for about 13.6% of the total energy loss; while the conduction loss caused by heat dissipation takes up around 2%, and the rest five losses (including radiant losses of the mental foam and the surface of the inner cylinder) around 1.4%.

The reflective property of the quartz glass material and shape of the quartz glass window are two dominant influencing factors on the reflective loss of the quartz glass window, of which the latter substantially influences the reflective efficiency. Generally, paraboloid-shaped or cylindrical-typed quartz glass windows generate less reflective loss than the flat one. However, to lower cost and structural complexity, the flat one was chosen as the shape of quartz glass window in the experiment. High-quality quartz glass may reduce the reflectivity to about 7%. Hence, the reflective loss could be reduced by means of material improvement in future design.

Heat insulation and temperature distribution on the outer surface of the receiver are two dominant influencing factors on heat dissipation, of which the former is mainly influenced by thermal insulation materials, leaving little room for improvement. Temperature distribution depends on chamber structure and heat transfer structure, and improvement in the internal heat transfer structure may effectively curtail heat dissipation.

The radiation-induced heat loss is mainly influenced by chamber temperature. As long wave accounts for the major part of chamber radiation, and the quartz glass bears high reflectivity and absorptivity for long wave radiation, the radiation from the chamber is limited. In this case, radiant loss is controllable.

3.3. Model application

This simplified heat transfer model is highly conducive to solar receiver design as it is capable of estimating energy efficiency and heat loss. Its application may cover: the initial design before fabrication, fast performance prediction of different geometries for optimization, or the performance prediction of a given geometry under available conditions that experiments cannot reach. Heat loss analysis plays a key role in identifying major loss sources and presenting directions and suggestions for potential improvement and optimization.

The proposed model has broad prospects in application. The flow temperature at the rear of the solar receiver is crucial since it could be considered as the temperature of the hot end of a cycle, which in turn defines the cycle efficiency. Therefore, a higher outlet

temperature is desired. One possible method is to enhance the inlet air temperature by adding a recuperator in front of the solar receiver inlet. In the present experiment, however, heat regenerator is absent as the experimental instruments and conditions are limited, the inlet air temperature is thus relatively low. Therefore, the performance of the solar receiver with high inlet temperature could be well predicted with this model.

The calculated values of air mass flux and incident solar radiation are identical with the experimental ones. The inlet temperature used in the model was from experimental measurement, whereas a rough estimation of outlet temperature was set as the initial value. The calculation was converged after 100 interactions. Simulations were performed under five varying working conditions, where inlet temperature ranged from 44 °C to 463 °C, and the results are listed in Figs. 6–8. The result of Case 1 is exactly the same with that of the experiment, whereas no experimental data is available for the other four cases with higher inlet air temperature.

Fig. 6 depicts variation of energy efficiency against the mean temperature (Tm). A decreasing trend of energy efficiency is identified due to heat loss increment caused by high operation temperature. Specifically, the energy efficiency is around 82.3% when the mean experiment temperature reaches 250 °C, yet the number

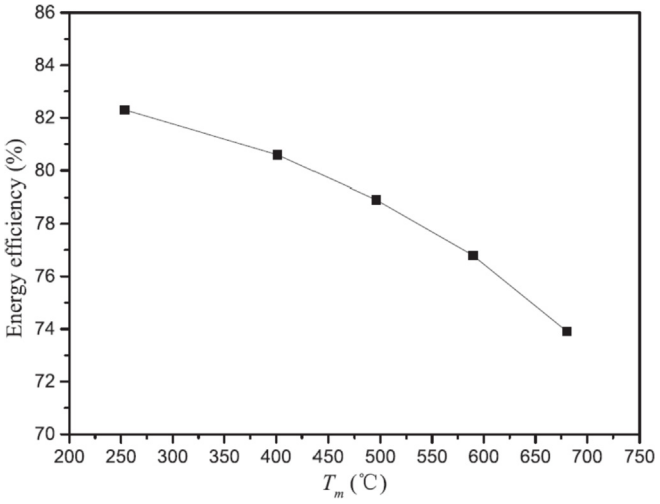

Fig. 6. Variation of energy efficiency against mean temperature.

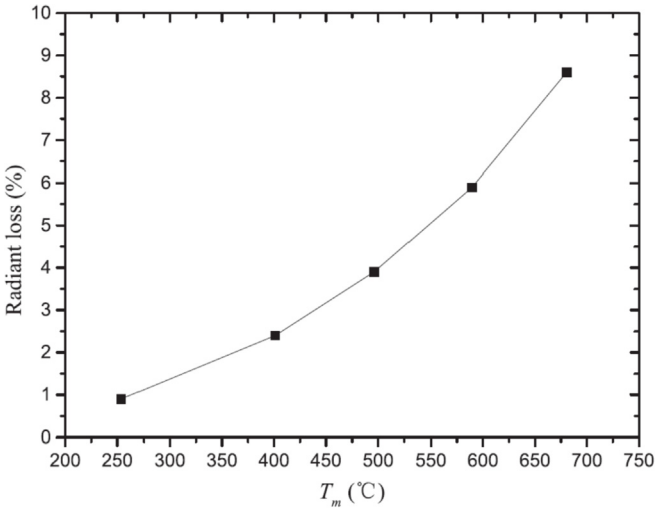

Fig. 7. Variation of radiant loss against mean temperature.

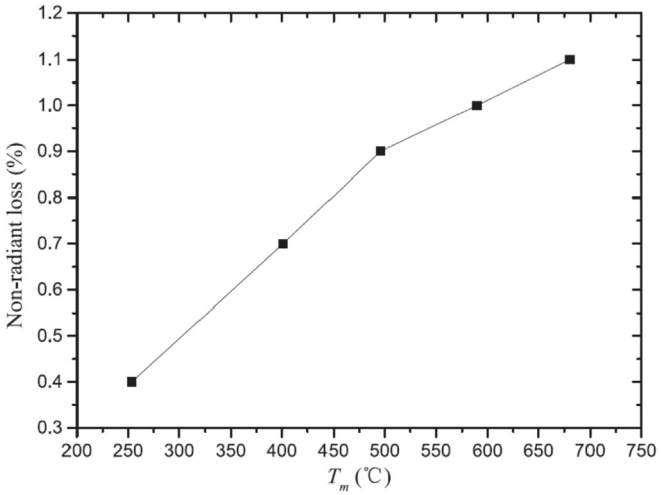

Fig. 8. Variation of non-radiant loss against Tm.

reduced to 73.9% when the mean temperature increased to 680.5 °C. The higher the mean temperature, the larger the absolute value of the slope. It is anticipated that further increase in the mean temperature acetates decline of the energy efficiency. The radiant loss, in contrast, is elevating with mean temperature increment (see Fig. 7). Consisting of emissive loss of the quartz glass, metal foam, and inner cylinder surface, radiant loss takes up around 0.9% of the total energy loss in the experiment (Case 1), and rocks to 8.6% at the highest operation temperature. It can be concluded that the energy efficiency could be further improved in case of radiant loss reduction. Besides, the corresponding curve slope is increasing as the radiation magnitude augments according to the power law. Non-radiant heat loss mainly concerns the natural convection loss of the quartz glass. Fig. 8 uncovers that although non-radiant heat loss is increasing with T_m, the growth speed is dropping off. Accounting for merely less than 1.1% of the total energy loss in all the simulated cases, non-radiant heat loss could be neglected in a wide range of inlet air temperature.

4. Conclusions

This work presents a heat transfer model for solar receiver with metal foam by virtue of thermal computation and value comparison (with the available experimental data). Several heat transfer processes, including forced convection, natural convection, heat conduction and radiation, are analyzed. This model can be used for prediction of energy efficiency and percentage contribution of each form of heat loss. The results reveal good agreement between the predicted results and the experimental data. Further prediction of the performance of the solar receiver was carried out in the conditions out of the range of the experiments. It is concluded that inlet air temperature increment of the solar receiver may result in energy performance degradation and increase of radiant heat loss. Yet non-radiant heat loss accounts for less than 1.1% of the total energy loss in all the simulated cases, indicating that the energy efficiency could be further improved in case of radiant loss reduction.

Acknowledgement

The authors are grateful for the financial support from Royal Academy of Engineering (DVF1718\8\26), United Kingdom.

References

[1] Zhu J, Kai W, Wu H, Wang D, Du J, Olabi AG. Experimental investigation on the energy and exergy performance of a coiled tube solar receiver. Appl Energy 2015;156:519–27. https://doi.org/10.1016/j.apenergy.2015.07.013.

[2] Roux WGL, Bello-Ochende T, Meyer JP. Operating conditions of an open and direct solar thermal Brayton cycle with optimized cavity receiver and recuperator. Energy 2011;36:6027–36. https://doi.org/10.1016/j.energy.2011.08.012.

[3] Kalogirou S. The potential of solar industrial process heat applications. Appl Energy 2003;76:337–61. https://doi.org/10.1016/s0306-2619(02)00176-9.

[4] Tian Y, Zhao CY. A review of solar collectors and thermal energy storage in solar thermal applications. Appl Energy 2013;104:538–53. https://doi.org/10.1016/j.apenergy.2012.11.051.

[5] Yao Z, Wang Z, Lu Z, et al. Modeling and simulation of the pioneer 1 MW solar thermal central receiver system in China. Renew Energy 2009;34(11):2437–46. https://doi.org/10.1016/j.renene.2009.02.022.

[6] Wang M, Siddiqui K. The impact of geometrical parameters on the thermal performance of a solar receiver of dish-type concentrated solar energy system. Renew Energy 2010;35:2501–13. https://doi.org/10.1016/j.renene.2010.03.021.

[7] Grange B, Ferriere A, Bellard D, Vrinat M, Couturier R, Pra F, et al. Thermal performances of a high temperature air solar absorber based on compact heat exchange technology. J Sol Energy Eng 2011;133:031004. https://doi.org/10.1115/1.4004356.

[8] Bader R, Pedretti A, Steinfeld A. Experimental and numerical heat transfer analysis of an air-based cavity-receiver for solar trough concentrators. J Sol Energy Eng 2012;134:519–28. https://doi.org/10.1115/1.4005447.

[9] Bader R, Barbato M, Pedretti A, Steinfeld A. An air-based cavity-receiver for solar trough concentrators. J Sol Energy Eng 2010;132:1–7. https://doi.org/10.1115/1.4001675.

[10] Wang K, Wu H, Wang D, Wang Y, Tong Z, Lin F, et al. Experimental study on a coiled tube solar receiver under variable solar radiation condition. Sol Energy 2015;122:1080–90. https://doi.org/10.1016/j.solener.2015.10.004.

[11] Wang Y, Wang K, Tong Z, Lin F, Nie C, Engeda A. Design and optimization of a single stage centrifugal compressor for a solar dish-brayton system. J Therm Sci 2013;22:404–12. https://doi.org/10.1007/s11630-013-0642-x.

[12] Karsli S. Performance analysis of new-design solar air collectors for drying applications. Renew Energy 2007;32(10):1645–60. https://doi.org/10.1016/j.renene.2006.08.005.

[13] Zhao CY. Review on thermal transport in high porosity cellular metal foams with open cells. Int J Heat Mass Transf 2012;55:3618–32. https://doi.org/10.1016/j.ijheatmasstransfer.2012.03.017.

[14] Calmidi VV, Mahajan RL. Forced convection in high porosity metal foams. J Heat Transf 2000;122:557–65. https://doi.org/10.1115/1.1287793.

[15] Mendes MAA, Ray S, Trimis D. An improved model for the effective thermal conductivity of open-cell porous foams. Int J Heat Mass Transf 2014;75(75):224–30. https://doi.org/10.1016/j.ijheatmasstransfer.2014.02.076.

[16] Kumar P, Topin F. Simultaneous determination of intrinsic solid phase conductivity and effective thermal conductivity of Kelvin like foams. Appl Therm Eng 2014;71(1):536–47. https://doi.org/10.1016/j.applthermaleng.2014.06.058.

[17] Buck R, BräUning T, Denk T, Pfander M, Schwarzbozl P, Tellez F. Solar-hybrid Gas turbine-based power tower systems (REFOS). J Sol Energy Eng 2002;124:2–9. https://doi.org/10.1115/1.1445444.

[18] Albanakis C, Missirlis D, Michailidis N, Yakinthos K, Goulas A, Omar H, et al. Experimental analysis of the pressure drop and heat transfer through metal foams used as volumetric receivers under concentrated solar radiation. Exp Therm Fluid Sci 2009;33:246–52. https://doi.org/10.1016/j.expthermflusci.2008.08.007.

[19] Michailidis N, Stergioudi F, Omar H, Missirlis D, Vlahostergios Z, Tsipas S, et al. Flow, thermal and structural application of Ni-foam as volumetric solar receiver. Sol Energy Mater Sol Cells 2013;109:185–91. https://doi.org/10.1016/j.solmat.2012.10.021.

[20] He YL, Xiao J, Cheng ZD, et al. A MCRT and FVM coupled simulation method for energy conversion process in parabolic trough solar collector. Renew Energy 2011;36(3):976–85. https://doi.org/10.1016/j.renene.2010.07.017.

[21] Wu Z, Wang Z. Fully coupled transient modeling of ceramic foam volumetric solar air receiver. Sol Energy 2013;89:122–33. https://doi.org/10.1016/j.solener.2012.12.016.

[22] Chen X, Xia XL, Meng XL, Dong XH. Thermal performance analysis on a volumetric solar receiver with double-layer ceramic foam. Energy Convers Manag 2015;97:282–9. https://doi.org/10.1016/j.enconman.2015.03.066.

[23] Hischier I. Experimental and numerical analyses of a pressurized air receiver for solar-driven gas turbines. J Sol Energy Eng 2012;134:021003. https://doi.org/10.1115/1.4005446.

[24] Hess D, Lipiski W, Modest M, Steinfeld A. Heat transfer analysis of a novel pressurized air receiver for concentrated solar power via combined cycles. J Therm Sci Eng Appl 2009;1:105–12. https://doi.org/10.1115/1.4001259.

[25] Hischier I, Poživil P, Steinfeld A. A modular ceramic cavity-receiver for high-temperature high-concentration solar applications. J Sol Energy Eng 2012;134:011004. https://doi.org/10.1115/1.4005107.

[26] Poživil Aga V, Zagorskiy A, Steinfeld A. A pressurized air receiver for solar-driven gas turbines. Energy Procedia 2014;49:498–503. https://doi.org/10.1016/j.egypro.2014.03.053.

[27] Lim S, Kang Y, Lee H, Shin S. Design optimization of a tubular solar receiver with a porous medium. Appl Therm Eng 2014;62:566–72. https://doi.org/10.1016/j.applthermaleng.2013.10.025.

[28] Weigel P. Development and piloting of a pressurized volumetric solar heat receiver designed to run with a Brayton cycle gas turbine. Leibniz University; 2013.

[29] Mortazavi B, Yang H, Mohebbi F, et al. Graphene or h-BN paraffin composite structures for the thermal management of Li-ion batteries: a multiscale investigation[J]. Appl Energy 2017;202:323–34. https://doi.org/10.1016/j.apenergy.2017.05.175.

[30] Röger M, Rickers C, Uhlig R, Neumann F, Polenzky C. Infrared-reflective coating on fused silica for a solar high-temperature receiver. J Sol Energy Eng Trans ASME May 2009;131(2). https://doi.org/10.1115/1.3097270. 0210041-0210047.

[31] Yang S, Tao W. Heat transfer. fourth ed. Beijing: Higher Education Press; 2012.

[32] Zhao CY, Kim T, Lu TJ, Hodson HP. Thermal transport in high porosity cellular metal foams. J Thermophys Heat Transf 2004;18:309–17. https://doi.org/10.2514/1.11780.

[33] Wong LT, Chow WK. Solar radiation model. Appl Energy 2001;69:191–224. https://doi.org/10.1016/s0306-2619(01)00012-5.